Inorganic Chemistry

Article

pubs.acs.org/IC

Zero-Field Splitting in a Series of Structurally Related Mononuclear Ni^{II}–Bispidine Complexes

Mihail Atanasov,*[,†,‡,§] Peter Comba,*[,†] Stefan Helmle,[†] Dennis Müller,[†] and Frank Neese*[,‡]

[†]Anorganisch-Chemisches Institut, Universität Heidelberg, INF 270, D-69120 Heidelberg, Germany

[‡]Max-Planck-Institut für Chemische Energiekonversion, Stiftstrasse 34-36, D-45470 Mülheim an der Ruhr, Germany

[§]Institute of General and Inorganic Chemistry, Bulgarian Academy of Sciences, 1113 Sofia, Bulgaria

Supporting Information

ABSTRACT: The synthesis, single-crystal X-ray structures, electronic absorption spectra, and magnetic properties of six Ni^{II} complexes with a tetradentate (L^1) and three pentadentate (L^2, L^3, L^4) bispidine ligands (3,7-diazabicyclo[3.3.1]nonane derivatives), $Ni(L^1{\cdot}H_2O)(OH_2)_2](PF_6)_2$, $[Ni(L^1{\cdot}H_2O)(O_2NO)]NO_3$, $[Ni(L^1{\cdot}H_2O)(OOCCH_3)]PF_6$, $[Ni(L^2{\cdot}H_2O)NCMe](PF_6)_2$, $[Ni(L^3{\cdot}H_2O)OH_2](PF_6)_2$, and $[Ni(L^4{\cdot}H_2O)NCMe](PF_6)_2$ are reported. The Ni–donor bonding to pyridine and tertiary amine groups and oxygen- or nitrogen-bound coligands, completing the octahedral coordination sphere of Ni^{II}, is analyzed using a combination of ab initio electronic structure calculations (complete active space self-consistent field, CASSCF, followed by N-electron valence perturbation theory, NEVPT2) and angular overlap ligand field analysis. Magnetic properties are rationalized with an analysis of the magnetic anisotropy in terms of zero-field splitting and *g*-tensor parameters, obtained from first principles, and their correlation with the Ni^{II}–donor bonding parameters from the ligand field analysis of the ab initio results. A two-dimensional spectrochemical series of the ligands considered, according to their σ and π bonding to Ni^{II}, is also derived.

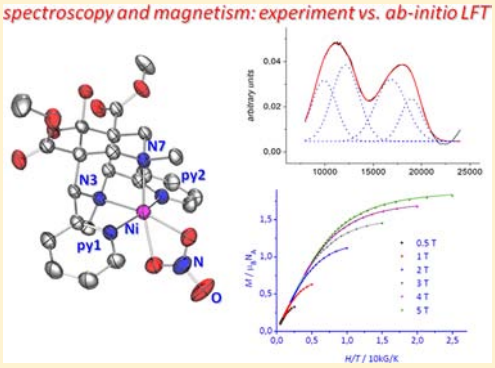

INTRODUCTION

A fundamental understanding of zero-field splitting (ZFS) is of importance in various areas of transition metal coordination chemistry, involving mono- and oligonuclear complexes of paramagnetic ions. Specifically in the field of molecular magnetism, where nanomagnets and in particular single-molecule magnets (SMMs) have attracted much attention in the past decade, the important electronic properties depend on the magnetic anisotropy D.[1−3] A thorough interpretation of spectroscopic parameters is also crucial for many applications in bioinorganic chemistry and catalysis. However, due to the small magnitude of the axial (D) and rhombic (E) ZFS parameters, accurate values and the sign of these parameters are often not easily accessible experimentally,[4−6] and only recently computational procedures have been described to efficiently and relatively accurately predict them.[4,7−11]

A particularly simple case of mononuclear transition metal compounds with a magnetic anisotropy, and therefore qualified for exploration and validation of methods for a theoretical analysis of the zero-field splitting, are Ni^{II} complexes with a triplet ground state (S = 1) and a 3- or 4-fold axial symmetry which in zero field leads to a splitting of the three sublevels into the doubly degenerated M_S = ±1 and M_S = 0 states. For hexacoordinate Ni^{II} complexes, a relatively large variation of the magnetic anisotropy D from −22.3[12] to +9.5 cm^{-1} [13] has been reported. The importance of a large and negative D for Ni^{II} fragments used as building blocks for oligonuclear SMMs has been emphasized,[14,15] and mechanisms leading to a positive or negative sign of D have been discussed.[4] For Ni^{II} complexes, eqs 1 and 2 for the zero-field splitting D and the g tensor, respectively, are valid[16,17]

$$E_{\pm1} - E_0 = D = k^2\zeta^2 \frac{\Delta E(^3B_2) - \Delta(^3E)}{\Delta E(^3B_2)\cdot\Delta(^3E)} \quad (1)$$

$$g_z = g_0 + \frac{4k^2|\zeta|}{\Delta E(^3B_2)};\ g_{x,y} = g_0 + \frac{4k^2|\zeta|}{\Delta E(^3E)} \quad (2)$$

with the spin–orbit coupling parameter ζ (SOC, ζ = −650 cm^{-1} for free Ni^{II}[18]), the orbital reduction factor k, and the electronic transitions $\Delta E(^3B_2)$ and $\Delta E(^3E)$ from the ground ($^3B_{1g}$) to the excited state split components $^3B_2$, ^3E (D_{4h} notation) of the parent octahedral $^3T_{2g}$ term. The angular overlap model (AOM) allows one to relate the energy difference $\Delta E(^3B_2) - \Delta E(^3E)$, i.e., the splitting of $^3T_{2g}$ due to the axial distortion, and therefore the sign of D, with the σ-donor and π-donor/acceptor properties of the axial (a) and equatorial (e) ligands, described by parameters e_σ^a, e_σ^e, e_π^a, e_σ^e (e_π > 0, π donor; e_π < 0, π acceptor). From eq 3 it follows that there are three main criteria which have an influence on the ZFS of Ni^{II} complexes: (i) the geometric distortion of the system

Received: July 25, 2012
Published: October 26, 2012

   dx.doi.org/10.1021/ic3016047 | *Inorg. Chem.* 2012, 51, 12324−12335

$$\Delta E(^3B_2) - \Delta(^3E) = (3/2)(e_\sigma^e - e_\sigma^a) + 2(e_\pi^a - e_\pi^e) \quad (3)$$

(D_{4h} symmetry or lower), (ii) the ligand field strength of the various donors, and (iii) the covalence of the in-plane and axial metal–ligand interactions k.[12] Therefore, the choice of ligand system allows one to carefully tune and control the magnitude of D.

Experimentally, the magnitude of D can be determined with a variety of methods, including electron paramagnetic resonance (EPR), magnetic susceptibility measurements, magnetic circular dichroism (MCD), and Mössbauer spectroscopy.[19] However, for an explicit determination of the sign of D, high-field EPR (HF-EPR) is the most adequate method.[20] Since this is not a routine technique, it is important to develop reliable computer-based models to determine the sign and magnitude of the ZFS. Theoretical analysis of the anisotropy in transition metal complexes requires ab initio[21−25] or DFT methods[26] to calculate the spin-dependent part of the energy. Two dominant contributions are (i) a dipolar term which arises from the spin–spin interaction between two pairs of electrons[22] and (ii) spin–orbit coupling which mixes ground and excited states which differ in spin by $\Delta S = \pm 1,0$. Through this mixing SOC reintroduces some orbital momentum into the electronic ground state which otherwise is quenched by low symmetry. Recent results demonstrate the possibility of ab initio methods to predict with experimental accuracy both the sign and the magnitude of the ZFS parameters[23−25,27] and show the limitations of DFT-based methods.

We report a series of six Ni^{II} complexes of the tetra- and pentadentate bispidine-type ligands L^1–L^4 (see Chart 1) with the general formula $[Ni(L^n)(X)_m](PF_6)_y$ (X = H_2O, m = 2 or 1 for L^1 or L^3; X = NO_3^-, m = 1 for L^1; X = CH_3COO^-, m = 1 for L^1; X = CH_3CN, m = 1 for L^2 and L^4). The whole set of structures could be solved experimentally, and the magnetic properties are characterized by magnetic susceptibility and field-dependent isothermal magnetization measurements. On the basis of the crystallographic data and DFT geometry-optimized structures an ab initio method[24,25] was applied to interpret the experimental results. Magneto-structural correlations are shown to allow an explicit analysis of the relation between D and the Ni–ligand bonding in these complexes.

Chart 1. Structure and Numbering of the Ligands

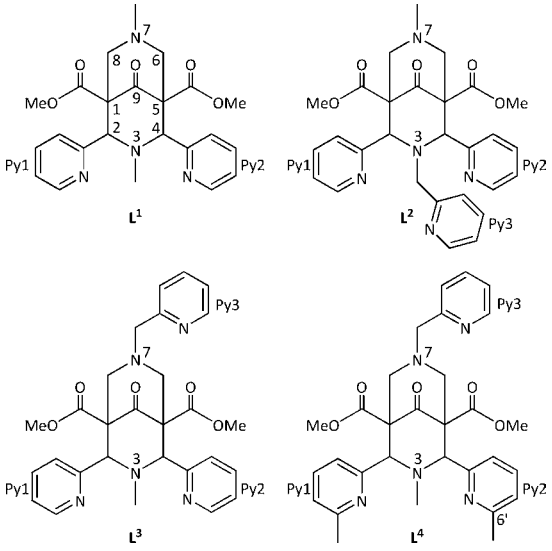

RESULTS AND DISCUSSION

Syntheses and Structural Properties. The syntheses of the Ni^{II} complexes involved Ni^{II} perchlorate or tetrafluoroborate salts and the bispidine ligands L^1–L^4. By addition of an excess of NH_4PF_6, pink to violet crystals of the hexafluorophosphate complexes, adequate for structural analysis, could be obtained. Single crystals of $[Ni(L^1{\cdot}H_2O)(O_2NO)]NO_3$ could be obtained from reaction of $Ni(NO_3)_2$ with L^1. $[Ni(L^1{\cdot}H_2O)(OOCCH_3)]PF_6$ was obtained from a solution of $Ni(OOCCH_3)_2{\cdot}4H_2O$ and the ligand L^1, and single crystals for X-ray analysis were obtained after addition of NH_4PF_6. Crystal and structural refinement data are given as Supporting Information, ORTEP plots of the structurally analyzed complex cations are shown in Figure 1, and selected structural data are listed in Table 1.

The characteristic structural data of the Ni^{II}–bispidine complexes are all in the expected range (specifically also the N3···N7 distances (2.862–2.923 Å) and M–N bond lengths).[28] With the exception of $[Ni(L^4{\cdot}H_2O)(NCMe)](PF_6)_2$, all complexes have as usual a long axis along the N7–Ni bond, which varies from 2.106(4) Å for $[Ni(L^1{\cdot}H_2O)$-

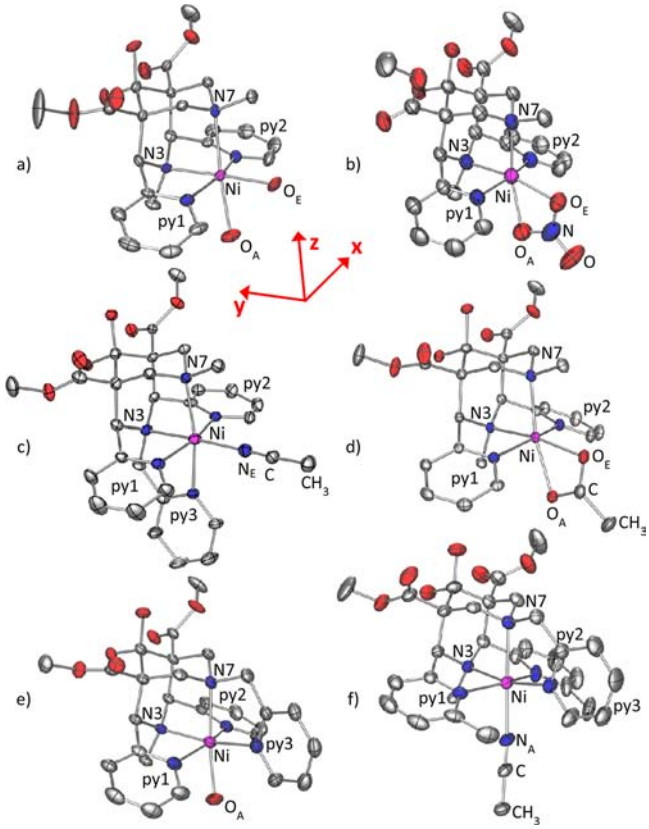

Figure 1. Plots of the molecular cations of the X-ray structures of (a) $[Ni(L^1{\cdot}H_2O)(OH_2)_2]^{2+}$, (b) $[Ni(L^1{\cdot}H_2O)O_2NO]^+$, (c) $[Ni(L^2{\cdot}H_2O)$-$(NCMe)]^{2+}$, (d) $[Ni(L^1{\cdot}H_2O)(OOCCH_3)]^+$, (e) $[Ni(L^3{\cdot}H_2O)$-$(OH_2)]^{2+}$, and (f) $[Ni(L^4{\cdot}H_2O)(NCMe)]^{2+}$ showing 30% probability ellipsoids and the atom labeling. Hydrogen atoms have been omitted for clarity; for the sake of the ligand field analysis the following set of Cartesian axes has been chosen: z is parallel to the Ni–N7 bond, the y axis has been calculated as a vector product between z and the Ni–Npy2 bond vector, and, finally, the x axis was taken as the vector product between the y and z vectors. For such a choice it follows that z exactly coincides with Ni–N7, while y and x are approximately parallel to the Ni–N3 and N(py1)–Ni–N(py2) bond directions.

dx.doi.org/10.1021/ic3016047 | Inorg. Chem. 2012, 51, 12324–12335

Table 1. Selected Structural Data: Experimental and DFT Geometry Optimized (italics) Results[a,j] of $[Ni(L^1{\cdot}H_2O)(OH_2)_2](PF_6)_2$, $[Ni(L^1{\cdot}H_2O)O_2NO]NO_3$, $[Ni(L^1{\cdot}H_2O)(OOCCH_3)]PF_6$, $[Ni(L^2{\cdot}H_2O)NCMe](PF_6)_2$, $[Ni(L^3{\cdot}H_2O)OH_2](PF_6)_2$, and $[Ni(L^4{\cdot}H_2O)NCMe](PF_6)_2$

	$[Ni(L^1{\cdot}H_2O)(OH_2)_2](PF_6)_2$	$[Ni(L^1{\cdot}H_2O)O_2NO]NO_3$	$[Ni(L^1{\cdot}H_2O)(OOCCH_3)]PF_6$	$[Ni(L^2{\cdot}H_2O)NCMe](PF_6)_2$[b]	$[Ni(L^3{\cdot}H_2O)OH_2](PF_6)_2$	$[Ni(L^4{\cdot}H_2O)NCMe](PF_6)_2$
Ni–N(3)	2.078(3) *2.080*	2.042(3) *2.067*	2.058(2) *2.081*	2.066(3)/2.096(3) *2.097*	2.087(3) *2.107*	2.073(3) *2.113*
Ni–N(7)	2.174(3) *2.167*	2.106(4) *2.140*	2.126(3) *2.162*	2.214(4)/2.192(3) *2.243*	2.179(4) *2.167*	2.176(3) *2.173*
$Ni–N_{Py1}$	2.081(3) *2.035*	2.055(3) *2.048*	2.083(3) *2.052*	2.062(4)/2.081(3) *2.081*	2.073(5) *2.033*	2.175(4) *2.162*
$Ni–N_{Py2}$	2.040(3) *2.021*	2.079(3) *2.034*	2.084(3) *2.046*	2.102(4)/2.081(3) *2.065*	2.050(5) *2.084*	2.240(4) *2.316*
$Ni–X_E$[c]	2.071(3)[d] *2.145*	2.102(3)[e] *2.117*	2.074(2)[f] *2.106*	2.051(4)/2.067(4)[g] *1.977*	2.043(4)[h] *2.032*	2.054(4)[h] *2.057*
$Ni–X_A$[i]	2.134(3)[d] *2.247*	2.166(4)[e] *2.215*	2.147(2)[f] *2.186*	2.125(4)/2.092(4)[h] *2.089*	2.140(4)[d] *2.204*	2.085(4)[g] *2.014*
N(3)···N(7)	2.893 *2.925*	2.862 *2.908*	2.871 *2.910*	2.923/2.907 *2.945*	2.914 *2.936*	2.870 *2.918*
σ[k]	0.06	0.04	0.04	0.02/0.04	0.04	0.05
N(3)–Ni–N(7)	85.7(1) *87.0*	87.2(1) *87.4*	86.65(9) *86.6*	86.1(1)/ 85.4(1) *85.4*	86.2(2) *86.8*	84.9(1) *85.5*
$N(3)–Ni–N_{Py1}$	81.1(1) *82.2*	81.9(1) *82.0*	80.61(10) *81.7*	81.1(1)/ 82.3(1) *81.6*	81.2(2) *81.1*	78.1(2) *79.6*
$N(3)–Ni–N_{Py2}$	81.7(1) *82.1*	81.5(1) *82.1*	80.97(10) *81.6*	81.7(1)/ 80.9(1) *81.0*	81.2(2) *80.4*	80.3(1) *77.6*
$N(3)–Ni–X_E$	177.4(1) *174.7*	167.3(2) *168.4*	170.12(9) *169.3*	176.7(2)/ 177.5(2) *178.4*	169.2(2) *168.5*	166.8(2) *167.7*
$N(3)–Ni–X_A$	98.4(1) *100.3*	106.4(1) *108.2*	108.03(9) *107.4*	83.8(1)/ 83.7(1) *83.4*	98.7(2) *99.4*	98.5(1) *97.4*
σ[k]	1.9	1.1	0.8	1.0 1.0	0.7	1.7

[a]Distances in Angstroms, angles in degrees, with estimated standard deviations in parentheses. [b]There are two crystallographically independent structures in the unit cell. [c]Coordination site trans to N(3). [d]Bonded to OH_2. [e]Bonded to O_2NO (bidentate). [f]Bonded to O_2CCH_3 (bidentate). [g]Bonded to $NCCH_3$. [h]Bonded to N-pyridyl. [i]Coordination site trans to N7. [j]PBE functional, van der Waals corrections for nonbonding interactions (VDW10); ZORA; def2-TZVP basis set (def2-TZVP/J auxiliary basis); COSMO. [k]Standard deviations (σ) between experimental and calculated (DFT-optimized) distances and angles.

$(O_2NO)]NO_3$ to 2.214 Å for $[Ni(L^2{\cdot}H_2O)(NCMe)](PF_6)_2$.[29] The N3–Ni–$X_E$ axis tends to be shorter with a bond length for N3–Ni between 2.042(3) Å for $[Ni(L^1{\cdot}H_2O)(O_2NO)]NO_3$ and 2.096(3) Å for the Ni2 site in $[Ni(L^2{\cdot}H_2O)(NCMe)](PF_6)_2$. Therefore, the Ni^{II} complexes of L^1–L^3 can be described as elongated octahedral with quasi-D_{4h} symmetry. In contrast, $[Ni(L^4{\cdot}H_2O)(NCMe)](PF_6)_2$ has a compressed octahedral geometry with long axes along N_{py1}–Ni–N_{py2} (on average 2.208 Å) and N7–Ni–X_A (2.131 Å) and a short axis along N3–Ni–X_E (Ni–N3 = 2.064 Å). This change in the coordination geometry arises from the two methyl groups in the C6′ position of the pyridyl groups py1 and py2. The steric demand of the methyl substituents leads to an elongation of the N_{py1}–Ni–N_{py2} axis and, due to the small size of the acetonitrile coligand, to a contraction of the Ni–N_A bond distance (2.085(4) Å). A comparison of the two complexes with acetonitrile as monodentate coligand ($[Ni(L^2{\cdot}H_2O)(NCMe)](PF_6)_2$ and $[Ni(L^4{\cdot}H_2O)(NCMe)](PF_6)_2$) indicates that most of the bond distances are similar, with the important exception of the Ni–$N_{py1/2}$ bonds with 2.082 vs 2.208 Å on average. These structural differences induce striking differences in the electronic and magnetic properties and are the basis for the study presented here. With the tetradentate bispidine ligand L^1, three structures with important differences were obtained: in contrast to $[Ni(L^1{\cdot}H_2O)(OH_2)_2](PF_6)_2$, the two species with chelating coligands $[Ni(L^1{\cdot}H_2O)(O_2NO)]NO_3$ and $[Ni(L^1{\cdot}H_2O)(OOCCH_3)]PF_6$ have a strongly distorted coordination sphere, with X_E–Ni–X_A angles of 60.9(1)° and 62.13(10)° vs 80.9(1)° for $[Ni(L^1{\cdot}H_2O)(OH_2)_2](PF_6)_2$. Furthermore, there are significant differences in the Ni–N3 and Ni–N7 distances. These features also lead to significantly different magnetic behavior.

Spectroscopy and Magnetism. Electronic absorption spectra of the Ni^{II} complexes (Figure 2) display two broad and structured bands assigned to the two spin-allowed d–d transitions $^3A_{2g} \rightarrow {}^3T_{2g}$ and $^3A_{2g} \rightarrow {}^3T_{1g}$ (F). An additional d–d transition due to the formally two-electron excitation $^3A_{2g} \rightarrow {}^3T_{1g}$ (P) appears as a shoulder of the charge transfer

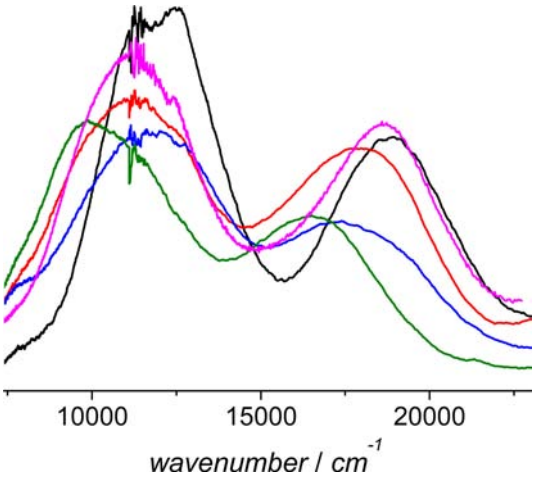

Figure 2. Diffuse reflectance absorption spectra of the d–d transitions (F term) of (red line) $[Ni(L^1{\cdot}H_2O)(O_2NO)]NO_3$, (purple line) $[Ni(L^1{\cdot}H_2O)(OOCCH_3)]PF_6$, (black line) $[Ni(L^2{\cdot}H_2O)(NCMe)](PF_6)_2$, (blue line) $[Ni(L^3{\cdot}H_2O)(OH_2)](PF_6)_2$, and (green line) $[Ni(L^4{\cdot}H_2O)(NCMe)](PF_6)_2$.

transition at around 30 000 cm^{-1} (see Supporting Information). Due to the reduced symmetry (pseudo-D_{4h}), the $^3T_{2g}$ and $^3T_{1g}$ (F and P) terms are split into B_{2g}, E_g, and $^3A_{2g}$ as well as ^3E_g, respectively. Therefore, the expected bands in the visible part of the electronic absorption spectra are at least doubled. Except for $[Ni(L^2{\cdot}H_2O)(NCMe)](PF_6)_2$, this splitting is resolved in this series of Ni^{II} complexes. The lowest energy transitions (derived from $^3T_{2g}$ and $^3T_{1g}$ (F), Figure 2) were simulated with Gaussian functions (see Supporting Information). As shown in the spectrum of $[Ni(L^2{\cdot}H_2O)(NCMe)](PF_6)_2$ (Figure 3), excellent fits are observed with three Gaussian envelopes.

The six N-donor ligands with similar ligand field strength of $[Ni(L^2{\cdot}H_2O)(NCMe)](PF_6)_2$—two tertiary amines (pure σ donors), three pyridine groups (σ donor and weak π donor), and MeCN (σ donor and π acceptor)—induce a ligand field of close to octahedral symmetry, and this is consistent with a very

dx.doi.org/10.1021/ic3016047 | Inorg. Chem. 2012, 51, 12324–12335

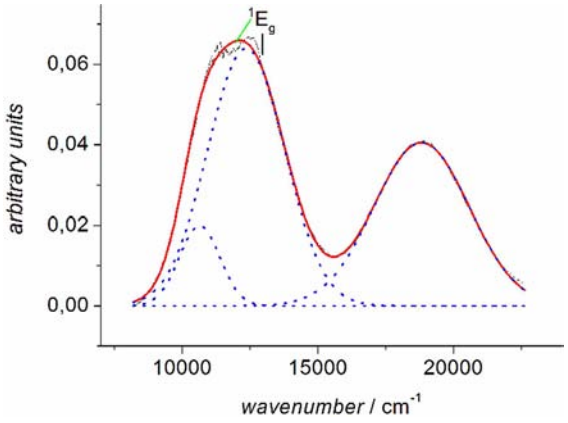

Figure 3. Experimental solid-state diffuse reflectance absorption spectrum of the d−d transitions (F term) of (—) $[Ni(L^2{\cdot}H_2O)(NCMe)](PF_6)_2$ and its simulation with three Gaussian envelopes (see Supporting Information for more detail). d−d transition energies from the simulation are 10 640, 12 363, and 18 824 cm^{-1}.

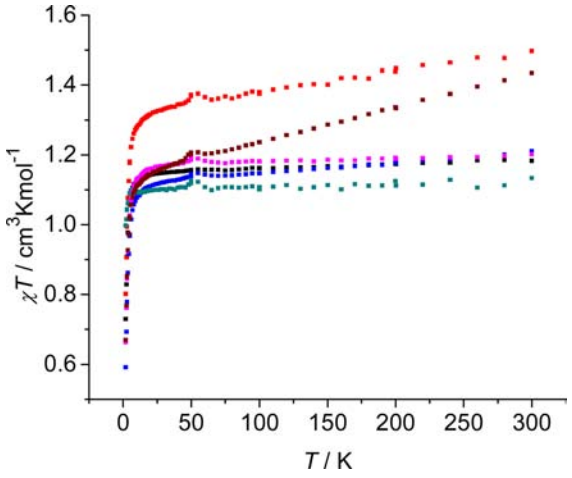

Figure 4. χT vs T plot of (black squares) $[Ni(L^1{\cdot}H_2O)(OH_2)_2](PF_6)_2$, (red squares) $[Ni(L^1{\cdot}H_2O)(O_2NO)]NO_3$, (brown squares) $[Ni(L^1{\cdot}H_2O)(OOCCH_3)]PF_6$, (green squares) $[Ni(L^2{\cdot}H_2O)(NCMe)](PF_6)_2$, (blue squares) $[Ni(L^3{\cdot}H_2O)(OH_2)](PF_6)_2$, and (purple squares) $[Ni(L^4{\cdot}H_2O)(NCMe)](PF_6)_2$.

low ZFS (see magnetic properties). Simulation of the electronic spectra of all other Ni^{II} complexes was done with four Gaussian envelopes, since the transitions around 20 000 cm^{-1} are clearly asymmetric. From these deconvolutions (see Table 2) it emerges that $[Ni(L^2{\cdot}H_2O)(NCMe)](PF_6)_2$ exhibits the highest transition energies with 10 640 ($^3A_{2g} \rightarrow {}^3T_{2g}$ (F)) and 18 800 cm^{-1} ($^3A_{2g} \rightarrow {}^3T_{1g}$ (F)), while $[Ni(L^4{\cdot}H_2O)(NCMe)](PF_6)_2$ has the lowest ligand field with corresponding transitions at 9445, 10 500 cm^{-1} ($^3A_{2g} \rightarrow {}^3T_{2g}$ (F)) and 15 200, 17 000 cm^{-1} ($^3A_{2g} \rightarrow {}^3T_{1g}$ (F)), and this reflects to a large extent the structural observations (see above).

Magnetic susceptibilities were measured from powdered crystals of the complexes at 500 G in the temperature range of 2−300 K (Figure 4). With the exception of $[Ni(L^1{\cdot}H_2O)(O_2NO)]NO_3$ and $[Ni(L^1{\cdot}H_2O)(OOCCH_3)]PF_6$ the values for χT at room temperature are all in a narrow range of 1.133−1.210 cm^3 K mol^{-1}, consistent with a spin-triplet (S = 1) ground state and a g value slightly larger than the g factor of the free electron. The room-temperature χT values of $[Ni(L^1{\cdot}H_2O)(O_2NO)]NO_3$ and $[Ni(L^1{\cdot}H_2O)(OOCCH_3)]PF_6$ are 1.497 and 1.434 cm^3 K mol^{-1}, respectively, significantly larger. This may be attributed to the larger distortion of these two complexes, leading to a stronger mixing of the ground and excited states, and a pseudo-D_{4h} description may therefore not be adequate. Due to a significantly stronger TIP, a clearly ascending χT value is visible at higher temperatures. The

Table 2. Experimental and Calculated[a] d−d Transitions[b,c] (in cm^{-1}) of $[Ni(L^1{\cdot}H_2O)(OH_2)_2](PF_6)_2$, $[Ni(L^1{\cdot}H_2O)O_2NO]NO_3$, $[Ni(L^2{\cdot}H_2O)NCMe](PF_6)_2$, $[Ni(L^1{\cdot}H_2O)(OOCCH_3)]PF_6$, $[Ni(L^3{\cdot}H_2O)OH_2](PF_6)_2$, and $[Ni(L^4{\cdot}H_2O)NCMe](PF_6)_2$[d]

complex	^3E_g	$^3B_{2g}$	$^1B_{1g}/{}^1A_{1g}$	$^3A_{2g}$(F)	^3E_g(F)	$^3A_{2g}$(P)	^3E_g(P)
$[Ni(L^1{\cdot}H_2O)(OH_2)_2](PF_6)_2$	*11 509 [11 614]*	*13 399 [13 306]*	*15 266 [15 171]*	*19 184 [18 619]*	*21 373 [20 665]*	*30 463 [31 479]*	*31 770 [31 785]*
	11 984 [12 519]		*15 995 [16 092]*		*21 388 [21 291]*		*32 532 [32 158]*
$[Ni(L^1{\cdot}H_2O)(O_2NO)]NO_3$	9910	12 132	~12 600	16 828	18 963	~29 900 (sh)	~29 900
	11 359 [10 528]	*12 919 [13 500]*	*15 441 [15 226]*	*18 099 [17 533]*	*20 307 [20 216]*	*29 194 [28 972]*	*31 202 [31 301]*
	11 418 [11 756]		*15 867 [16 086]*		*21 251 [21 824]*		*32 041 [31 925]*
$[Ni(L^1{\cdot}H_2O)(OOCCH_3)]PF_6$	10 228	12 290	~12 500	15 314	18 550	~28 400 (sh)	~28 400 (sh)
	11 091 [10 371]	*12 362 [13 146]*	*15 614 [15 355]*	*17 671 [16 936]*	*19 549 [19 717]*	*28 892 [28 548]*	*30 515 [30 764]*
	11 393 [11 258]		*15 904 [16 169]*		*21 033 [21 530]*		*31 667 [31 556]*
$[Ni(L^2{\cdot}H_2O)(NCMe)](PF_6)_2$	10 640	12 363	~11 900	18 824		~30 000 (sh)	~30 000 (sh)
Ni−site 1	*12 005 [11 530]*	*13 372 [14 098]*	*15 830 [15 366]*	*20 255 [19 016]*	*20 921 [19 910]*	*32 040 [32 977]*	*31 507 [30 947]*
	12 548 [12 308]		*15 887 [16 364]*		*21 124 [21 757]*		*31 774 [32 234]*
Ni-site 2	*12 538 [11984]*	*12 916 [13 818]*	*15 729 [15 453]*	*20 297 [18 746]*	*21 142 [203 78]*	*32 160 [33 096]*	*31 678 [31 374]*
	12 715 [12 583]		*15 930 [16 212]*		*21 190 [21 639]*		*31 962 [32 332]*
$[Ni(L^3{\cdot}H_2O)(OH_2)](PF_6)_2$	10 570	12 856		16 959	19 278	~30 000 (sh)	~30 000 (sh)
	11 234 [11 539]	*13 940 [13 951]*	*14 792 [14 724]*	*19 144 [18 450]*	*21 094 [20 611]*	*30 849 [30 883]*	*31 818 [31 987]*
	11 834 [12 113]		*15 964 [16 035]*		*21 443 [21 553]*		*32 223 [32 433]*
$[Ni(L^4{\cdot}H_2O)(NCMe)](PF_6)_2$	9445	10 477	~11 600	15 204	16 999	~27 300 (sh)	~27 300 (sh)
	9844 [9740]	*12 598 [13 224]*	*15 169 [15 100]*	*19 906 [19 666]*	*18 088 [17 500]*	*30 643 [31 160]*	*29 119 [29 208]*
	10 950 [11 134]		*15 865 [15 935]*		*18 475 [18 407]*		*29 697 [29 345]*

[a]Italics: NEVPT2. Italics, square brackets: fitted with values from Table 5, see text. [b]Gaussian analysis, see text and Supporting Information. [c]Term energies calculated using the AOM (square brackets) use B and C from Table 5. [d]Term notations in D_{4h} pseudosymmetry

dx.doi.org/10.1021/ic3016047 | Inorg. Chem. 2012, 51, 12324−12335

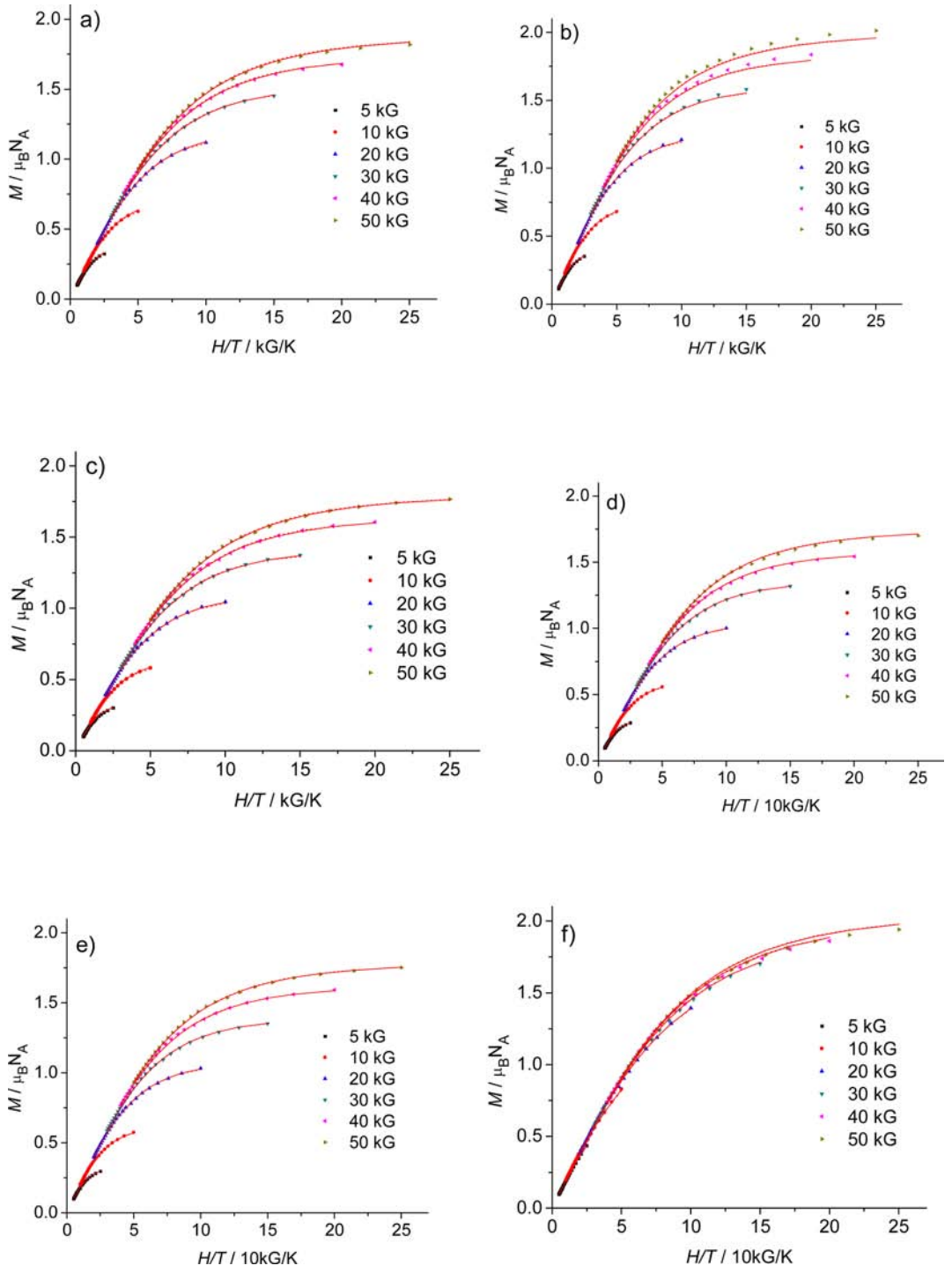

Figure 5. Field dependence of the reduced magnetization of (a) $[Ni(L^1{\cdot}H_2O)(OH_2)_2](PF_6)_2$, (b) $[Ni(L^1{\cdot}H_2O)(O_2NO)]NO_3$, (c) $[Ni(L^1{\cdot}H_2O)(OOCCH_3)]PF_6$, (d) $[Ni(L^3{\cdot}H_2O)(OH_2)](PF_6)_2$, (e) $[Ni(L^4{\cdot}H_2O)(NCMe)](PF_6)_2$, (f) $[Ni(L^2{\cdot}H_2O)(NCMe)](PF_6)_2$ (symbols, experimental data; red lines, set of parameters for negative D; dotted lines, set of parameters for positive D (both reproduce the experimental data equally well); see also Table 3).

bidentate coligands nitrate and acetate also induce an increased orbital reduction factor k.[30] At low temperature (ca. 15 K) the χT values for all compounds strongly decrease, and this is attributed to a significant zero-field splitting. It is not unexpected that with $[Ni(L^2{\cdot}H_2O)(NCMe)](PF_6)_2$, which is expected to exhibit a much smaller ZFS (see above), a strikingly different behavior is observed.

Magnetization measurements were carried out at different magnetic field strengths (5000−50 000 G) in the temperature range of 2−10 K (see Figure 5). Magnetization vs H/T plots of the Ni^{II} complexes indicate a moderate zero-field splitting. Best-fit parameters for the axial (D) and orthorhombic (E) ZFS parameters and the effective g-tensor values obtained from simulations of the magnetic data with the spin Hamiltonian of eq 4 (where $B = B_x, B_y, B_z$ is the magnetic flux density and μ_B is the Bohr magneton) are listed in Table 3. Except for $[Ni(L^2{\cdot}H_2O)(NCMe)](PF_6)_2$, the D values vary only slightly and $[Ni(L^2{\cdot}H_2O)(NCMe)](PF_6)_2$ shows the expected weaker

dx.doi.org/10.1021/ic3016047 | Inorg. Chem. 2012, 51, 12324−12335

Table 3. Best-Fit Values (simulations of the reduced magnetizations) of g, D, and E and Room-Temperature χT values, In Comparison to Calculated (NEVPT2) Values of D and E

		g_{av}[a]		D[b] [cm^{-1}]		E/D[b]	
	χT (300 K) [cm^3 K mol^{-1}]	fit	calcd	fit	calcd	fit	calcd
$[Ni(L^1{\cdot}H_2O)(OH_2)_2](PF_6)_2$	1.182	2.17	2.18	−4.07	4.19	0.333	0.07
		2.17		4.04	*4.76*	0.000	*0.09*
$[Ni(L^1{\cdot}H_2O)(O_2NO)]NO_3$	1.497	2.45	2.19	−4.47	5.35	0.333	0.20
		2.45		4.41		0.174	
$[Ni(L^1{\cdot}H_2O)(OOCCH_3)]PF_6$	1.434	2.39	2.20	−4.68	4.96	0.333	0.33
		2.39		4.61		0.173	
$[Ni(L^2{\cdot}H_2O)(NCMe)](PF_6)_2$[c]	1.133	2.13	2.18	−2.10	2.2	*d*	0.31
		2.13	2.25	1.85	2.07	*d*	0.16
$[Ni(L^3{\cdot}H_2O)(OH_2)](PF_6)_2$	1.210	2.20	2.18	−4.88	4.38	0.333	0.19
		2.20		4.84		0.280	
$[Ni(L^4{\cdot}H_2O)(NCMe)](PF_6)_2$	1.201	2.19	2.21	−4.91	5.51	0.333	0.30
		2.19		4.86		0.268	

[a]Values of g_{av} are obtained from a fit to the T = 300 K values of χT, calculated from the main values of the g tensor (NEVPT2) g_e, g_m, and g_h and $g_{av}^2 = (g_e^2 + g_m^2 + g_h^2)/3$. [b]Results for D and E obtained using the sum-overstates method in combination with second-order perturbation theory are given in italics. [c]Two crystallographically independent structures in the unit cell. [d]No distinctive value could be obtained.

ZFS (reduction by more than 50%). While excellent fits of the magnetization data were obtained, the sign of D is, as often is observed, not unambiguous. Therefore, the next section reports ab initio results combined with a ligand field analysis to try to resolve these ambiguities.

$$H = D[\hat{S}_z^2 - S(S+1)] + E(\hat{S}_x^2 - \hat{S}_y^2) + g\mu_B(\hat{S}_x B_x + \hat{S}_y B_y + \hat{S}_z B_z) \quad (4)$$

DFT and ab Initio Results. *Complex Geometries from DFT Geometry Optimizations.* The six complexes were geometry optimized using the def2-TZVP basis sets, the resolution of identity (RI) option in ORCA,[31,32] the def2-TZVP/J auxiliary basis, the Perdew−Becke−Enzerhof (PBE) functional,[33,34] and an empirical van der Waals correction[35] for the DFT energy. With a positive charge of +1 (coordinated nitrate or acetate) or +2 (coordinated solvent molecules) charge compensation with a polarizable solvent continuum is crucial for realistic results. Without a solvation model, in $[Ni(L^1{\cdot}H_2O)(OH_2)_2](PF_6)_2$, e.g., one of the coordinated water molecules (the weakly bound axial OH_2) dissociates and interacts via hydrogen bonds with the equatorial OH_2 ligand; with the conductor-like solvent model COSMO this is prevented.[36] Selected computed structural data are compared to the X-ray data in Table 1 (see Supporting Information for further details and the coordinate files). There is generally excellent agreement between experimental and computed structures (≤0.06 Å for distances and ≤2° for valence angles). However, for some longer bonds, in particular, the axial Ni−N7 bonds, the deviations are somewhat larger. In the following, experimental structural data are used for calculation of d−d transitions and zero-field splitting tensors.

d−d Transitions. In Table 2 the computed d−d transition energies (NEVPT2 calculations) for all 6 complexes are compared with the experimentally observed data. As expected for axially elongated octahedral complexes of Ni^{II} (elongations along Ni−N7, except for $[Ni(L^4{\cdot}H_2O)(NCMe)](PF_6)_2$, see above), the lowest excited state $^3T_2$ is split with the expected $^3E < {}^3B_2$ energy order. According to eqs 1 and 3 a positive value of D [$E(M_s = 0) < E(M_s = \pm 1)$] is predicted for the five axially elongate complexes. The other structure, $[Ni(L^4{\cdot}H_2O)NCMe](PF_6)_2$, has two weak py1−Ni−py2 and N7−Ni−$NCCH_3$ and one strong N3−Ni−py ligand field directions, corresponding to a tetragonal compression (see above), and this leads to a $^3T_2$ splitting pattern with $^3E > {}^3B_2$. According to Table 2, however, the orthorhombic ligand field lifts all orbital degeneracies of ^3E in all six compounds. Its origin will be analyzed using a ligand field analysis of the ab initio results below. There is good agreement between experimental (deconvolution into Gaussian components) and NEVPT2 calculated energies of the d−d transitions. Due to some missing dynamic correlation (accounted by NEVPT2 to second order only) and/or basis set incompleteness, the energies of the d−d transitions tend to be overestimated by the post-Hartree−Fock calculations. Computed values are typically overestimated by less than 2000 cm^{-1} for spin-allowed transitions but may be less accurate for spin-forbidden transitions.[37] This is also reflected in the results of Table 2.

Spin-Hamiltonian Parameters. In contrast to complexes with $S > 1$ where there is a large ambiguity in the choice of a particular spin Hamiltonian, the Hamiltonian H_{ZFS} for the S = 1 Ni^{II} complexes (nondegenerate ground state, eq 5) is well defined. Here $\mathbf{D}$ and $\mathbf{g}$ are the (symmetric) ZFS tensor (eq 6) and $\mathbf{g}$ the (nonsymmetric) matrix, respectively. Within the basis of the spin functions $|S = 1, M_S\rangle$, M_S = 1,0,−1, H_{ZFS} takes the form of eq 7.

$$H_{spin} = H_{ZFS} + H_{Zeeman} = \vec{S}\mathbf{D}\vec{S} + \mu_B\vec{B}\mathbf{g}\vec{S} \quad (5)$$

$$\mathbf{D} = \begin{bmatrix} D_{xx} & D_{xy} & D_{xz} \\ D_{xy} & D_{yy} & D_{yz} \\ D_{xz} & D_{yz} & D_{zz} \end{bmatrix} \quad (6)$$

$$H_{ZFS} = \begin{array}{c} \\ |1,1\rangle \\ |1,0\rangle \\ |1,-1\rangle \end{array} \begin{array}{c} \begin{array}{ccc} |1,1\rangle & |1,0\rangle & |1,-1\rangle \end{array} \\ \begin{bmatrix} (1/2)(D_{xx}+D_{yy})+D_{zz} & (1/\sqrt{2})(D_{xz}-iD_{yz}) & (1/2)(D_{xx}-D_{yy})-iD_{xy} \\ (1/\sqrt{2})(D_{xz}+iD_{yz}) & D_{xx}+D_{yy} & (1/\sqrt{2})(-D_{xz}+iD_{yz}) \\ (1/2)(D_{xx}-D_{yy})+iD_{xy} & (1/\sqrt{2})(-D_{xz}-iD_{yz}) & (1/2)(D_{xx}+D_{yy})+D_{zz} \end{bmatrix} \end{array} \quad (7)$$

It follows from eq 7 that there are 6 independent matrix elements (or 5 if the approximation of a preserved barycenter is used, $D_{xx} + D_{yy} + D_{zz} = 0$), i.e., the same number as parameters defining $\mathbf{D}$. With H_{ZFS} reduced to a diagonal form, the usual

dx.doi.org/10.1021/ic3016047 | Inorg. Chem. 2012, 51, 12324−12335

Table 4. Zero-Field Splitting D_{ij} ($i, j = x, y, z$, in cm^{-1}) and g_i (i = easy (e), medium (m), and hard (h)) Tensor Parameters from First-Principles (NEVPT2) Calculations Obtained via 1:1 Mapping of the Spin-Hamiltonian Parameters to the Model Space of the Three Lowest SOC-Split $S = 1$ Spin Sublevels of the Electronic Ground State of the Ni^{II} Bispidine Complexes

	$[Ni(L^1{\cdot}H_2O)(OH_2)_2](PF_6)_2$[a]	$[Ni(L^1{\cdot}H_2O)O_2NO]NO_3$	$[Ni(L^1{\cdot}H_2O)(OOCCH_3)]PF_6$	$[Ni(L^2{\cdot}H_2O)(NCMe)](PF_6)_2$[b] Ni1 Ni2	$[Ni(L^3{\cdot}H_2O)(OH_2)](PF_6)_2$	$[Ni(L^4{\cdot}H_2O)(NCMe)](PF_6)_2$
D_{xx}	−1.45; *-1.72*	−0.71	−0.18	−0.02/−0.40	−0.61	3.29
D_{yy}	−0.65; *-0.70*	−1.24	−1.30	−1.41/−0.94	−2.24	−3.11
D_{zz}	2.10; *2.42*	1.95	1.48	1.42/1.34	2.86	−0.18
D_{xy}	0.36; *0.44*	−0.15	−0.57	−0.03/0.20	0.15	−1.51
D_{xz}	0.99; *1.06*	0.08	0.49	0.24/0.11	0.35	−0.31
D_{yz}	1.18; *1.32*	2.79	2.89	0.01/0.28	0.36	0.42
D_e	−1.71; *−2.00*	−2.87	−3.30	−1.46/−1.03	−2.28	−3.49
D_m	−1.09; *−1.18*	−0.70	0.01	0.06/−0.35	−0.64	−0.18
D_h	2.80; *3.17*	3.57	3.31	1.41/1.38	2.92	3.67
g_e	2.20‖$py_{1,2}$	2.21‖N3(y)	2.22‖N3(y)	2.19/2.26‖N3(y)	2.20‖N3(y)	2.24‖N3(y)
g_m	2.19‖N3(y)	2.20‖$py_{1,2}$	2.20‖$py_{1,2}$	2.18/2.25‖$py_{1,2}$	2.19‖$py_{1,2}$	2.21‖N7(z)
g_h	2.16‖N7(z)	2.16‖N7(z)	2.17‖N7(z)	2.17/2.24‖N7(z)	2.16‖N7(z)	2.18‖$py_{1,2}$
α_e[c]	5.3	4.3	3.4	0.9/10.0	1.8	1.0
α_m[c]	6.3	3.3	2.2	3.0/10.0	2.2	1.2
α_h[c]	5.3	3.1	3.2	3.0/0.7	1.5	0.9

[a]Zero-field splitting tensor values from a sum-overstate procedure based on second-order perturbation theory are given in italics. [b]Two crystallographically independent Ni sites. [c]Angles between the main axes of the ZFS and g tensors are given in degrees.

relations between the parameters D, E and D_{xx}, D_{yy}, and D_{zz} apply (eq 8). The ZFS parameters D_{ij}

$$D_{xx(yy)} = -(1/3)D + (-)E;\ D_{zz} = (2/3)D \tag{8}$$

are obtained by a 1:1 mapping,[22] following a published formalism.[38−41] This is readily done by a comparison of eq 7 with the 3 × 3 matrix resulting from the projection of the SOC-split $^3A_2$ ground state (calculated within the CASSCF CI vectors and their NEVPT2 diagonally corrected eigenvalues) onto the model space of the ground state $|S = 1, M_S\rangle$, $M_S = 1, 0, -1$ sublevels (full details of one example are given as Supporting Information). A similar procedure is applied to extract the elements of the g matrix from the ORCA output (diagonal form, see ref 42). The $\boldsymbol{D}$ and $\boldsymbol{g}$ tensors are defined in a molecular axes system with z parallel to Ni−N7 and y and x approximately parallel to Ni−N3 and Ni−py1,2, respectively (see Figure 1). ZFS and $\boldsymbol{g}$-tensor parameters for all complexes are listed in Table 4.

In the given Cartesian frame the $\boldsymbol{D}$ tensor is off-diagonal with matrix elements correlated to the Ni−L bonding directions. Therefore, the largest and positive diagonal element D_{ii} (implying a hard magnetic anisotropy direction) closely follows the weakest Ni−L bond, i.e., Ni−N7 (D_{zz}), in the five axially elongated complexes or Ni−py1,2 (D_{xx}) in the axially compressed complex. The largest and negative value of D, defining an easy magnetic anisotropy direction (D_e), correlates with the strongest Ni−L bond, i.e., it switches from Ni−N$py_{1,2}$ (D_{xx}) in $[Ni(L^1{\cdot}H_2O)(OH_2)_2](PF_6)_2$ to Ni−N3 (D_{yy}) in the other five compounds. Superimposed to this hard-axis/easy-plane magnetic anisotropy is a rather strong orthorhombic splitting, as also emerges from the splitting of the d−d energy levels (see Table 2). Eigenvalues and eigenfunctions of the $\boldsymbol{D}$ matrix—the latter are, apart from a change of sign, identical to the eigenvalues of eq 7—allow one to identify the easy, intermediate, and hard directions of the $\boldsymbol{D}$ tensors (D_e, D_m, D_h) and correlate them with the strength of the Ni−ligand interactions (see below). The eigenvalues of $\boldsymbol{D}$ (D_e, D_m, D_h) allow one to deduce values of E and D (eq 9, Table 3) and directly compare them to experimental data. They compare well with their values from the simulation of the magnetic data but also allow fixing the sign of D. In particular, the comparatively small D and E in $[Ni(L^2{\cdot}H_2O)(NCMe)](PF_6)_2$ (close to regular octahedral, see above) and the large orthorhombic E value [close to the limiting value of $(1/3)D$] for $[Ni(L^3{\cdot}H_2O)(OH_2)](PF_6)_2$ and $[Ni(L^4{\cdot}H_2O)(NCMe)](PF_6)_2$ are well reproduced.

$$D = D_h - (D_e + D_m)/2;\ E = (D_m - D_e)/2 \tag{9}$$

Importantly, the magnetic anisotropies deduced from the main values of the $\boldsymbol{g}$ tensor reflect consistently those emerging from the $\boldsymbol{D}$-tensor anisotropy. The two tensors $\boldsymbol{D}$ and $\boldsymbol{g}$ are not strictly collinear, but in all complexes the angles between their respective easy, intermediate, and hard axes directions are very small (the largest angles are 5−6° in $[Ni(L^1{\cdot}H_2O)(OH_2)_2](PF_6)_2$).

ZFS tensors of transition metal complexes with non-degenerate ground states have traditionally been calculated from first principles using sum-overstates formulas based on second-order perturbation theory (PT2, see Supporting Information; in addition to the usual expressions[43] effects of spin-flip excitations were also taken into account, see also refs 21 and 22). The method discussed here is different: it is based on effective Hamiltonian theory, and the results in Table 4 are of variational quality and therefore correct "to all orders". In Table 3 the values of D for $[Ni(L^1{\cdot}H_2O)(OH_2)_2](PF_6)_2$ are compared with those obtained by the sum-overstates method. The two sets of data differ significantly. Even in the standard case of a distorted octahedral complex of Ni^{II}, PT2 leads to an overestimate of D by up to 20% compared to the values obtained by the 1:1 mapping procedure.

Ligand-Field Analysis of the ab Initio Results. The database derived from the NEVPT2 calculations (Table 2) is a good starting point for ligand field analysis. The angular overlap model (AOM)[44−48] has a number of advantages over other parametrization schemes and, in particular, is based on general models of chemical bonding and therefore is appealing for chemists. In the AOM, the general matrix element of the one-electron (5 × 5) ligand field matrix for d orbitals (d_{xy}, d_{yz}, d_{z2},

dx.doi.org/10.1021/ic3016047 | Inorg. Chem. 2012, 51, 12324−12335

d_{xz}, d_{x2-y2}) is expressed as the sum of energies e_σ and e_π of each ligand perturbing the metal d orbitals in a standard orientation optimal for σ and π overlap, and angular factors account for a general ligand position which might violate the optimal alignment between the metal 3d and the ligand orbitals. The geometric factors are accounted for accurately based on a known complex geometry. This leaves the user with two parameters (e_σ and e_π) for each ligand−metal type to be adjusted from experiment or from quantum-chemical calculations. The high potential of this model in interpreting and understanding results from multireference electronic multiplet calculations of transition metal complexes was recently demonstrated.[24,25] With the three different donors of the bispidine ligands discussed here, coordinated to Ni^{II} (the tertiary amines (N7,N3), the pyridine groups (Npy1,Npy2), and one or two additional coligands X, trans to N3 (X_E) or N7 (X_A), see Table 1), there are three e_σ/e_π parameters sets. A general ab initio based ligand field model has been devised to extract such parameters from multireference CASSCF/NEVPT2 results.[25] However, even with this approach, the AOM is overparameterized in the series of complexes studied here, and this prevents a unique set of ligand field parameters from a direct fit to the ab initio results. More specifically, the results from such a fit are sensitive to the set of starting parameters employed in the fitting procedure. To circumvent this difficulty, NEVPT2 calculations of tetracoordinate homoleptic Ni^{II} model complexes with each of the relevant ligands were performed (see Supporting Information for the computed structures).

In these calculations a constant Ni−L bond distance (R = 2.07 Å) appropriate for octahedral Ni^{II} was used. The number of AOM bonding parameters is reduced with amines (the tertiary amines N3 and N7) which have no π interactions (e_π = 0), and with the pyridine nitrogen and the OH_2 oxygen donors there is a single π-bonding parameter ($e_{\pi s}$) which describes the interaction of the out-of-plane ligand π orbitals with Ni^{II}. The effect of the other coligands, O_2NO^-, $O_2CCH_3^-$, and $NCCH_3$, is parametrized with the usual set of e_σ, e_π values of linear donor groups. The resulting parameters and multiplet energies which reproduce the NEVPT2 results with remarkable accuracy are given as Supporting Information. A two-dimensional e_π vs e_σ plot (Figure 6) allows one to characterize the donor groups in the ligands discussed here with respect to their σ- and π-donor

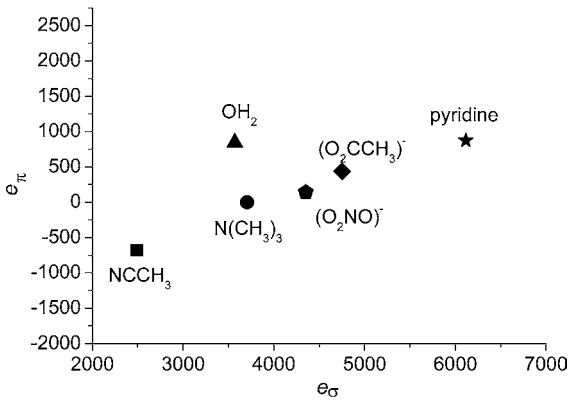

Figure 6. Two-dimensional spectrochemical series (AOM parameters e_π vs e_σ) of the donor groups relevant to the systems discussed; parameters derived from NEVPT2 calculations of the tetracoordinate Ni^{II} model complexes, R(Ni−X) = 2.07 Å.

character toward Ni^{II}. In terms of σ and π interactions, there are the expected variations (i.e., there is not a strictly linear correlation), but on average the series in increasing bond strengths follows the order $NCCH_3 < H_2O \cong N(CH_3)_3 < O_2NO \leq O_2CCH_3 <$ py.

The σ-bonding energy for $Ni^{II}[N(CH_3)_3]$ [e_σ = 3700 cm^{-1}] is in the range of electronic parameters deduced from spectroscopic data [3600−4600 cm^{-1}].[49] In agreement with earlier suggestions based on the interpretation of d−d spectra of *trans*-$[Ni(py)_4Cl_2]$ (e_π = 570 cm^{-1}) and $[Ni(py)_4Br_2]$ (e_π = 500 cm^{-1}),[50] pyridine acts as a weak π donor with Ni^{II}, and the parameters derived from experiment are close to those obtained by the NEVPT2-procedure used here (e_π = 800−900 cm^{-1}). The Ni−donor distances of the series of complexes analyzed here show a significant variation (see Table 1). To account for variations of bond distances with a specific metal−donor pair, a $1/R^n$ (n = 5−6) dependence of the AOM parameters on the distance has been empirically assumed for interpretation of ligand field spectra,[47,48,51,52] and this is also based on experimental studies of the dependence of the energies of d−d transitions on pressure.[53,54] Values of n_λ for an $e_\lambda = C_\lambda/R^{n\lambda}$ (λ = σ, π) distance dependence of the AOM parameters e_λ are given as Supporting Information. These have been deduced from the NEVPT2 calculations. While the n_σ values for II−V are in the expected range, this is not the case for I and VI. Interestingly, the e_π parameters are generally quite insensitive to variations of the bond distance. This may be a result from rehybridization of ligand orbitals in response to the increase of the Ni−ligand bond distance.

AOM parameter sets for each of the six mixed-ligand complexes have been determined (see Supporting Information) on the basis of transferability of AOM parameters and their described correlation with the Ni−ligand distance. With these parameters d−d transition energies were computed and are compared with experimental data in the Supporting Information. The overall agreement with experiment is good and even better than those of the NEVPT2 results, but the low-symmetry splitting deviates significantly from the initial NEVPT2 data (see Supporting Information). This may be due to some violation of the assumption of transferable ligand field parameters when extending the results of the homo- to the heteroleptic complexes. Therefore, we adopted an AOM parameter set (see Supporting Information) as starting input data for a fit to the NEVPT2 energies with two parameters (e_σ(py) and e_σ (X, X = OH_2, $NCCH_3$, O_2NO, O_2CCH_3) as well as B and C as variables and fixing the other parameters and parameter ratios at values given in the Supporting Information. The final set of this NEVPT2-consistent set of parameters for the mixed-ligand Ni^{II} bispidine complexes is listed in Table 5 with the corresponding d−d energies given for comparison in Table 2 .

There has been debate regarding the transferability of AOM parameters.[48,55−57] It follows from Table 5 that the e_σ parameters for Ni−$py_{bispidine}$ remain almost unchanged between the homoleptic model and the six mixed-ligand complexes, i.e., the parameters are largely transferrable. However, the σ-antibonding energies for the coligands (OH_2, O_2NO, O_2CCH_3, and $NCCH_3$) are significantly larger (by 1000−2000 cm^{-1}) in Ni^{II}−bispidine than in the model complexes. A possible reason is an increase of metal−ligand covalence induced by the Ni−pyridine polarity.[48] The variation of B (Table 5) is consistent with this interpretation, i.e., this indicates an increased covalency (nephelauxetic effect) in the bispidine complexes

dx.doi.org/10.1021/ic3016047 | *Inorg. Chem.* 2012, 51, 12324−12335

Table 5. e_σ and $e_{\pi s}$ (in brackets) AOM Parameters for the Ni–Donor Interactions of the Ni^{II}–Bispidine Complexes As Well As the Corresponding *B* and *C* Racah Parameters, Derived by Fitting to Electronic Term Energies from NEVPT2 Multireference Calculations (all parameters in cm^{-1})[a]

complex	N3	N7	py_1	py_2	X_E[b]	X_A[b]	*B*/*C*
$[Ni(L^1{\cdot}H_2O)(OH_2)_2](PF_6)_2$	*3625*	*2797*	5675 (*875*)	6793 (*843*)	5758 (*843*)	4916 (*779*)	892/4664
			5830	*6978*	*3561*	*3042*	
$[Ni(L^1{\cdot}H_2O)(O_2NO)]NO_3$	*4007*	*3357*	5733 (*870*)	5159 (*875*)	6634 (*140*)	5679 (*139*)	861/4829
			6531	*5881*	*4020*	*3442*	
$[Ni(L^1{\cdot}H_2O)(OOCCH_3)]PF_6$	*3832*	*3180*	5421 (*876*)	5400 (*876*)	6937 (*425*)	5460 (*252*)	879/4809
			5780	*5755*	*4691*	*3692*	
$[Ni(L^2{\cdot}H_2O)(NCMe)](PF_6)_2$[c]	*3747*	*2519*	6759 (*871*)	5684 (*880*)	4737 (*-618*)	5150 (*885*)	877/4858
			6334	*5325*	*3114*	*4826*	
	3450	*2668*	5998 (*875*)	5998 (*875*)	4674 (*-678*)	5722 (*878*)	887/4738
			5830	*5830*	*2580*	*5559*	
$[Ni(L^3{\cdot}H_2O)(OH_2)](PF_6)_2$	*3536*	*2760*	6048 (*874*)	6690 (*869*)	6901 (*867*)	4125 (*774*)	871/4702
			6036	*6676*	*6886*	*2997*	
$[Ni(L^4{\cdot}H_2O)(NCMe)](PF_6)_2$	*3675*	*2782*	4419 (*895*)	3389 (*909*)	7410 (*870*)	4378 (*-676*)	897/4580
			3912	*2999*	*6560*	*2092*	

[a]Values in italics are derived from the model complexes (see Table 5) by adjusting the values to the crystallographically observed Ni^{II}–donor distances. [b]X_E and X_A are defined in Table 1. [c]Two crystallographically independent Ni^{II} sites.

when compared with the homoleptic model complexes. The pronounced enhancement of covalency observed for coligands X_E and X_A in the bispidine complexes might be of importance for catalytic activation of small organic molecules in transition metal bispidine complexes.[28,58−63]

From ligand field analysis it was pointed out that the trace of the AOM matrix (Tr_{AOM}), i.e., the sum of the $e_\sigma + e_{\pi s} + e_{\pi c}$ parameters (at least for Co^{II}, Ni^{II}, and Cu^{II}), is approximately constant (~22 000 cm^{-1}) regardless of the ligand, coordination number, and geometry.[48] Tr_{AOM} reflects the overall ligand-to-metal charge donation, and its near constancy may be regarded as an energetic equivalent of the electroneutrality principle. It was noted that Tr_{AOM} for various N-heterocyclic complexes of Cu^{II} is anomalously high (28 000 cm^{-1}).[64] Similarly high values of Tr_{AOM} for the bispidine complexes are deduced from the AOM interpretation of our first-principles results (see Figure 7). However, Tr_{AOM} varies significantly along the series with the smallest value calculated for $[Ni(L^4{\cdot}H_2O)(NCMe)](PF_6)_2$ with the rather bulky 6-CH_3-py substituents. This might suggest steric effects to be responsible for some of these variations. Decomposition of Tr_{AOM} into parts along the three directions Npy1–Ni–Npy2 ($Tr_{Npy1Npy2}$), N3–Ni–X_E ($Tr_{N3\text{-}XE}$), and N7–Ni–X_A ($Tr_{N7\text{-}XA}$) (Figure 7) shows as expected that the strongest Ni–ligand interactions are along the Npy1–Ni–Npy2 bonds in the five axially enlongated bispidine complexes but change to N3–Ni–X_E in $[Ni(L^4{\cdot}H_2O)(NCMe)](PF_6)_2$ with a tetragonally compressed geometry. With one exception (N3–Ni–X_E in $[Ni(L^2{\cdot}H_2O)(NCMe)](PF_6)_2$), the N7–Ni–$X_A$ interactions are the weakest. Except for $[Ni(L^4{\cdot}H_2O)(NCMe)](PF_6)_2$, with D_h parallel to py1,2, this is also the direction of the hard anisotropy axis and therefore correlated with the large and positive *D* value. Finally, all three energies $Tr_{Npy1Npy2}$, $Tr_{N3\text{-}XE}$, and $Tr_{N7\text{-}XA}$ differ significantly in all six complexes, but the largest difference occurs in $[Ni(L^4{\cdot}H_2O)(NCMe)](PF_6)_2$ with a tetragonal compression, and this is also the complex with the largest *E* value. However, Figure 7 also indicates that there is not an unambiguous correlation between the Ni^{II}–donor interactions defined by the three energies $Tr_{Npy1Npy2}$, $Tr_{N3\text{-}XE}$, and $Tr_{N7\text{-}XA}$ and the hard, intermediate, and easy axes of the magnetic anisotropy, reflected by the eigenvalues of the ***D*** and ***g*** tensors (Table 4).

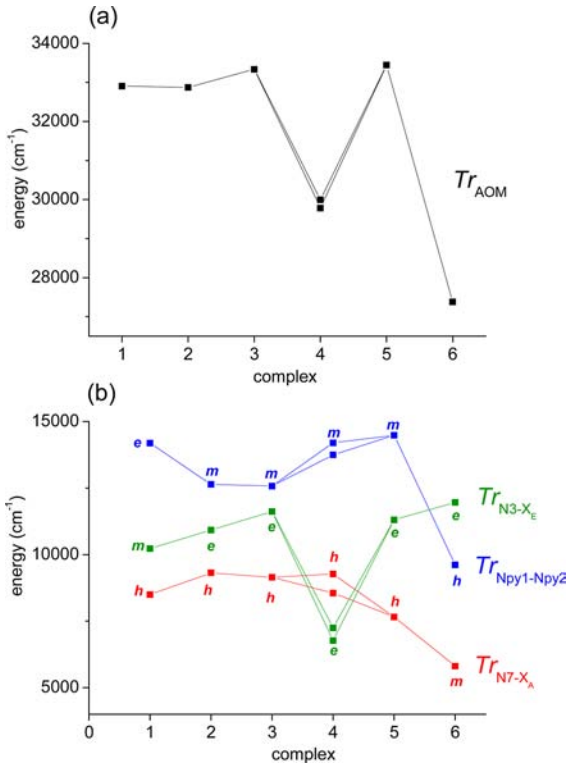

Figure 7. (a) Traces of the AOM matrices of the six bispidine complexes (1) $[Ni(L^1{\cdot}H_2O)(OH_2)_2](PF_6)_2$, (2) $[Ni(L^1{\cdot}H_2O)(O_2NO)]NO_3$, (3) $[Ni(L^1{\cdot}H_2O)(OOCCH_3)]PF_6$, (4) $[Ni(L^2{\cdot}H_2O)(NCMe)](PF_6)_2$, (5) $[Ni(L^3{\cdot}H_2O)(OH_2)](PF_6)_2$, and (6) $[Ni(L^4{\cdot}H_2O)(NCMe)](PF_6)_2$; (b) traces of the AOM matrices along the three distinguishable bond directions N3–Ni–X_E, Npy1–Ni–Npy2, and N7–Ni–X_E; the directions of the hard (h), medium (m), and easy (e) magnetic axes are also identified; both crystallographically independent Ni^{II} sites are indicated in the two plots.

CONCLUSIONS

Six Ni^{II} complexes with tetradentate (L^1) and pentadentate (L^2, L^3, L^4) bispidine ligands are reported and characterized by their crystal structures, optical d–d absorption spectra, and magnetic properties (magnetic susceptibilities and field as well as

dx.doi.org/10.1021/ic3016047 | Inorg. Chem. 2012, 51, 12324−12335

temperature-dependent reduced magnetizations). Spectroscopic and magnetic data are interpreted based on multireference ab initio CASSCF/NEVPT2 calculations. A largely anisotropic zero-field splitting tensor due to the spin−orbit/low-symmetry split $^3A_2$ complex ground state with a large and positive D and an also large orthorhombic parameter E emerge. The positive value of D and the large orthorhombicity reflected by the parameter E are the result of the three different ligands in the coordination sphere of Ni^{II}, two tertiary amines, two pyridine groups, and one or two coligands (OH_2, O_2NO^-, $O_2CCH_3^-$, and $NCCH_3$), leading to distorted structures with two (four) weak (strong) axial (equatorial) bonds superimposed by large low-symmetry structural distortions due to the bidentate ligands O_2NO^- and $O_2CCH_3^-$.

A two-dimensional series of the ligands according to their σ-donor and π-donor/acceptor functions toward Ni^{II} is deduced, based on NiL_4 model complexes by a least-squares fit of the angular overlap parameters to electronic multiplet energies from ab initio NEVPT2 calculations. The σ-donor character increases in the series $NCCH_3 < H_2O \cong N(CH_3)_3 < O_2NO \leq O_2CCH_3 <$ py. From the positive (pyridine) and negative ($NCCH_3$) values of e_π we can deduce that these two ligands interact with Ni^{II} as weak π donor and π acceptor, respectively.

From an angular overlap model analysis of the results from NEVPT2 multiplet calculations we conclude that AOM parameters for pyridine and tertiary amine are well transferrable from the single to the mixed-ligand complexes but the coligands OH_2, ONO_2^-, and $O_2CCH_3^-$ undergo a significant enhancement of their σ-donor character when coordinated to a $[Ni(bispidine)]^{2+}$ core. This might be of importance for the activation of small organic molecules by Ni−bispidine complexes.

EXPERIMENTAL SECTION

Measurements. *Powder UV−vis−NIR spectra.* Powder UV−vis−NIR spectra were recorded in Al_2O_3 with a V-570 UV−vis−NIR spectrophotometer (Jasco). Magnetic measurements were carried out on a MPMS-XL 5T (Quantum Design) SQUID magnetometer. Samples were powdered and pressed in PTFE tape to avoid field-induced orientation. Data were corrected for diamagnetism of the sample holder, and Pascal's constants were used for diamagnetic corrections of the sample.[65] Elemental analyses were obtained from the microanalytical laboratory of the Chemical Institutes of the University of Heidelberg.

X-ray Crystal Structure Determinations. Crystal data and details of structure determinations are given in the Supporting Information. Intensity data were collected at low temperature with a STOE IPDS1 image plate (Mo Kα radiation, graphite monochromator, λ = 0.71073 Å). Except for $[Ni(L^2{\cdot}H_2O)(NCMe)](PF_6)_2$ and $[Ni(L^1{\cdot}H_2O)(OOCCH_3)]PF_6$, absorption correction of the data from the IPDS was done numerically. Structures were solved by the heavy atom method and refined by full-matrix least-squares methods based on F^2 against all unique reflections.[66,67] All non-hydrogen atoms were given anisotropic displacement parameters. Most hydrogen atoms were input at calculated positions and refined with a riding model. Appropriate distance constraints were applied to the hydrogen atoms of the coordinated water of $[Ni(L^1{\cdot}H_2O)(OH_2)_2](PF_6)_2$. Structures frequently contained disordered solvent molecules (water and methanol). Whenever possible, these were included in the refined model. In some cases there was a rest of electron density, which could be assigned to solvent of crystallization. No hydrogen atoms could be located for the solvent water molecules of $[Ni(L^2{\cdot}H_2O)(NCMe)](PF_6)_2$ and $[Ni(L^3{\cdot}H_2O)(OH_2)](PF_6)_2$. The PF_6^- anions of all structures are partially disordered. CIF files for $[Ni(L^1{\cdot}H_2O)(OH_2)_2](PF_6)_2$, $[Ni(L^1{\cdot}H_2O)(O_2NO)]NO_3$, $[Ni(L^1{\cdot}H_2O)(OOCCH_3)]PF_6$, $[Ni(L^2{\cdot}H_2O)(NCMe)](PF_6)_2$, $[Ni(L^3{\cdot}H_2O)(OH_2)](PF_6)_2$, and $[Ni(L^4{\cdot}H_2O)(NCMe)](PF_6)_2$ are available as Supporting Information. CCDC 892832−892837 contain the crystallographic data of the structures reported here. These data can be obtained free of charge from The Cambridge Crystallographic Data Centre via www.ccdc.cam.ac.uk/data_request/cif.

Syntheses. *General and Ligands.* Chemicals were used as supplied. Technical-grade solvents were distilled prior to use. Ligands L^1, L^2, L^3, and L^4 were prepared as described previously.[68−71]

$[Ni(L^1{\cdot}H_2O)(OH_2)_2](PF_6)_2$. To L^1 (438 mg, 1 mmol) in 25 mL of methanol was added $Ni(BF_4)_2{\cdot}6H_2O$ (340 mg, 1 mmol) in 3 mL of water. The solution was stirred at 55 °C for 4 h and after cooling concentrated to one-half. Diethyl ether was slowly diffused into the solution, and after a few days a crude pink product could be obtained. Without further purification the product was solved in water and NH_4PF_6 (1.2 g, 7.4 mmol) was slowly added. The solution was filtrated, and after a few days at 4 °C pink crystals could be obtained. The pink product was washed with water and vacuum dried. Yield: 358 mg (43%). Anal. Calcd for $[Ni(L^1{\cdot}H_2O)(OH_2)_2](PF_6)_2$: C, 32.84; H, 3.83; N, 6.66. Found: C, 32.75; H, 3.85; N, 6.75.

$[Ni(L^1{\cdot}H_2O)(O_2NO)]NO_3$. To L^1 (438 mg, 1 mmol) in 25 mL of methanol was added $Ni(NO_3){\cdot}6H_2O$ (291 mg, 1 mmol) in 5 mL of methanol. The solution was stirred at 55 °C for 3 h and filtrated. The solution was concentrated to one-half, and diethyl ether was slowly diffused into the solution. Single crystals could be obtained after a few days. The purple product was vacuum dried. Yield: 435 mg (63%). Anal. Calcd for $[Ni(L^1{\cdot}H_2O)O_2NO]NO_3{\cdot}H_2O{\cdot}MeOH$: C, 41.82; H, 4.97; N, 12.19. Found: C, 41.79; H, 4.80; N, 12.44.

$[Ni(L^1{\cdot}H_2O)(OOCCH_3)]PF_6$. To L^1 (438 mg, 1 mmol) in 25 mL of methanol was added $Ni(OOCCH_3)_2{\cdot}4H_2O$ (249 mg, 1 mmol) in 5 mL of methanol. The solution was stirred at 55 °C for 4 h, and after cooling NH_4PF_6 (2 mmol, 325 mg) in 3 mL of water was added, and the solution was filtrated. Single crystals were obtained after a few days by slow evaporation of the solvent. The purple product was vacuum dried. Yield: 478 mg (65%). Anal. Calcd for $[Ni(L^1{\cdot}H_2O)(OOCCH_3)]PF_6{\cdot}H_2O$: C, 40.73; H, 4.51; N, 7.60. Found: C, 40.89; H, 4.58; N, 7.61.

$[Ni(L^2{\cdot}H_2O)(NCMe)](PF_6)_2$. To L^2 (355 mg, 0.69 mmol) in 7 mL of CH_3CN was added $Ni(BF_4)_2{\cdot}6H_2O$ (237 mg, ~0.69 mmol) in 3 mL of acetonitrile. The solution was heated to almost boiling temperature, and after cooling NH_4PF_6 in 5 mL of water (1.12 g, 6.9 mmol) was added. The solution was briefly heated and filtrated after cooling. Single crystals were obtained after a few days by slow evaporation of the solvent. The pale red product was vacuum dried. Yield: 350 mg (53%). Anal. Calcd for $[Ni(L^2{\cdot}H_2O)(NCMe)](PF_6)_2{\cdot}2H_2O$: C, 37.56; H, 3.99; N, 8.76. Found: C, 37.61; H, 3.89; N, 8.54.

$[Ni(L^3{\cdot}H_2O)(OH_2)](PF_6)_2$. To L^3 (516 mg, 1 mmol) in 20 mL of methanol was added $Ni(BF_4)_2{\cdot}6H_2O$ (340 mg, 1 mmol) in 3 mL of water. The solution was heated to almost boiling temperature, and after cooling NH_4PF_6 in 5 mL of water (1.63 mg, 10 mmol) was added. The solution was briefly heated and after cooling filtrated. Single crystals were obtained after a few days by slow evaporation of the solvent. The pale purple product was vacuum dried. Yield: 553 mg (60%). Anal. Calcd for $[Ni(L^3{\cdot}H_2O)(OH_2)](PF_6)_2{\cdot}H_2O$: C, 36.62; H, 3.84; N, 7.63. Found: C, 36.62; H, 4.00; N, 7.55.

$[Ni(L^4{\cdot}H_2O)(NCMe)](PF_6)_2$. To L^4 (1 g, 1.84 mmol) in 10 mL of methanol was added $Ni(ClO_4)_2{\cdot}6H_2O$ (673 mg, 1.84 mmol) in 3 mL of water. The solution was heated to almost boiling temperature, and the solvent was removed under reduced pressure. The crude product was solved in 20 mL of acetonitrile, and NH_4PF_6 in 10 mL of acetonitrile (1.50 g, 9.2 mmol) was added. The solution was concentrated to one-half, and diethyl ether was slowly diffused into the solution. Single crystals could be obtained after a few days. The purple product was vacuum dried. Yield: 1.17 g (68%). Anal. Calcd for $[Ni(L^4{\cdot}H_2O)NCMe](PF_6)_2$: C, 41.18; H, 3.89; N, 9.00. Found: C, 41.23; H, 4.14; N, 8.90.

Computation of the Electronic Energy Levels and Fitting of the Zero-Field Splitting Parameters from Magnetic Data. Ground and excited state energies and wave functions as well as magnetic properties were calculated with geometries from X-ray diffraction data or using the geometries of the model complexes I−VI

dx.doi.org/10.1021/ic3016047 | Inorg. Chem. 2012, 51, 12324−12335

(see Supporting Information) and the CASSCF module of ORCA (to account for static correlation) together with the *N*-electron valence perturbation theory (NEVPT2) (to account for dynamic correlation). In these correlated calculations, basis sets of def2-TZVPP, def2-TZVP, def2-SVP, and def2-TZVP(-f) quality for Fe, N, H, and C, respectively, alongside with the corresponding auxiliary sets have been used (see ref 31 and sample input files in the Supporting Information). For the simulation of the iso-field lines from the reduced magnetization data the program julX was used (Bill, E. at the Max-Plank Institute of Bioinorganic Chemistry, Mülheim Ruhr, Germany, MPI für Bioanorganische Chemie, Mülheim, Germany, http://www.mpibac.mpg.de/bac/logins/bill/julX_en.php). From these simulations parameters g_{av}, *D*, and *E*/*D* of Table 3 have been deduced.

■ ASSOCIATED CONTENT

Supporting Information

This material is available free of charge via the Internet at http://pubs.acs.org.

■ AUTHOR INFORMATION

Corresponding Author

*E-mails: peter.comba@aci.uni-heidelberg.de (P.C.); mihail.atanasov@cec.mpg.de.de (M.A.); frank.neese@cec.mpg.de (F.N.).

Notes

The authors declare no competing financial interest.

■ ACKNOWLEDGMENTS

Financial support by the German Science Foundation (DFG) is gratefully acknowledged.

■ REFERENCES

(1) Sessoli, R.; Gatteschi, D.; Caneschi, A.; Novak, M. A. *Nature* **1993**, *365*, 141.
(2) Sessoli, R.; Gatteschi, D. *Angew. Chem., Int. Ed.* **2003**, *42*, 243.
(3) Gatteschi, D.; Sessoli, R.; Villain, J. *Molecular Nanomagnets*; Oxford University Press: Oxford, 2006.
(4) Boca, R. *Coord. Chem. Rev.* **2004**, *248*, 757.
(5) Bakac, A. *Physical Inorganic Chemistry-Principles, Methods and Models*; Wiley: New York, 2010.
(6) Scott, R. A.; Lukehart, C. M. *Applications of Physical Methods to Inorganic and Bioinorganic Chemistry*; Wiley: New York, 2007.
(7) Solomon, E. I.; Scott, R. A.; King, R. B. *Computational Inorganic and Bioinorganic Chemistry*; Wiley: New York, 2009.
(8) Liakos, D. G.; Ganyushin, D.; Neese, F. *Inorg. Chem.* **2009**, *48*, 10572.
(9) Maurice, R.; Sivalingam, K.; Ganyushin, D.; Guihery, N.; De Graaf, C.; Neese, F. *Inorg. Chem.* **2011**, *50*, 6229.
(10) Atanasov, M.; Comba, P.; Hanson, G. R.; Hausberg, S.; Helmle, S.; Wadepohl, H. *Inorg. Chem.* **2011**, *50*, 6890.
(11) Atanasov, M.; Comba, P.; Helmle, S. *Inorg. Chem.* **2012**, *51*, 9357.
(12) Boca, R.; Dlhan, L.; Haase, W.; Herchel, R.; Maslejova, A. *Chem. Phys. Lett.* **2003**, *373*, 402.
(13) Boca, R.; Baran, P.; Dlhan, L.; Hvastijová, M.; Wltschek, G. *Chem. Phys. Lett.* **1998**, *284*, 254.
(14) Atanasov, M.; Comba, P.; Daul, C. A. *Inorg. Chem.* **2008**, *47*, 2449.
(15) Atanasov, M.; Comba, P.; Hausberg, S.; Martin, B. *Coord. Chem. Rev.* **2009**, *253*, 2306.
(16) Abragam, A.; Bleaney, B. *Electron Paramagnetic Resonance of transition Ions*; Clarendon Press: Oxford, 1970.
(17) Neese, F.; Solomon, E. I. In *Magnetoscience-From Molecules to Materials*, Miller, J. S., Drillon, M., Eds.; Wiley-VCH: Weinheim, 2003; Vol. *IV*.
(18) Figgis, B. N. *Nature* **1958**, *182*, 1958.
(19) Que, L., Jr. *Physical Methods in Bioinorganic Chemistry, Spectroscopy and Magnetism*; University Science Books: Sausalito, CA, 2000.
(20) Savitsky, A.; Möbius, K. *Photosynth. Res.* **2009**, *102*, 311.
(21) Neese, F.; Solomon, E. I. *Inorg. Chem.* **1998**, *37*, 6568.
(22) Neese, F. *J. Am. Chem. Soc.* **2006**, *128*, 10213.
(23) Neese, F.; Pantazis, D. A. *Faraday Discuss.* **2011**, *148*, 229.
(24) Atanasov, M.; Ganyushin, D.; Pantazis, D. A.; Sivalingam, K.; Neese, F. *Inorg.Chem.* **2011**, *50*, 7640.
(25) Atanasov, M.; Ganyushin, D.; Sivalingam, K.; Neese, F. *Struct. Bonding (Berlin)* **2012**, *43*, 149.
(26) Neese, F. *Coord. Chem. Rev.* **2009**, *253*, 526.
(27) Maganas, D.; Sottini, S.; Kyritsis, P.; Groenen, E. J. J.; Neese, F. *Inorg. Chem.* **2011**, *50*, 8741.
(28) Comba, P.; Kerscher, M.; Schiek, W. *Prog. Inorg. Chem.* **2007**, *55*, 613.
(29) Bleiholder, C.; Börzel, H.; Comba, P.; Ferrari, R.; Heydt, A.; Kerscher, M.; Kuwata, S.; Laurenczy, G.; Lawrance, G. A.; Lienke, A.; Martin, B.; Merz, M.; Nuber, B.; Pritzkow, H. *Inorg. Chem.* **2005**, *44*, 8145.
(30) Figgis, B. N. *Nature* **1964**, *203*, 1138.
(31) Neese, F. with contributions from Ute Becker, D. B.; Ganyushin, D.; Hansen, A.; Izsak, R.; Liakos, D. G.; Kollmar, C.; Kossmann, S.; Pantazis, D. A.; Petrenko, T.; Reimann, C.; Riplinger, C.; Roemelt, M.; Sandhöfer, B.; Schapiro, I.; Sivalingam, K.; Wennmohs, F.; Wezisla, B.; Kállay, M.; Grimme, S.; Valeev, E. *ORCA-An ab initio, DFT and semiempirical SCF-MO package*, Version 2.9; Mülheim a.d.R. The binaries of ORCA are available free of charge for academic users for a variety of platforms: Max.
(32) Neese, F. *Comput. Mol. Sci.* **2012**, *2*, 73.
(33) Perdew, J. P.; Burke, K.; Ernzerhof, M. *Phys. Rev. Lett.* **1996**, *77*, 3865.
(34) Perdew, J. P.; Burke, K.; Ernzerhof, M. *Phys. Rev. Lett.* **1997**, *78*, 1396 (Erratum).
(35) Grimme, S.; Antony, J.; Ehrlich, S.; Krieg, H. *J. Chem. Phys.* **2010**, *132*, 154104.
(36) Klamt, A.; Schürmann, G. *J. Chem. Soc., Perkin Trans. 2* **1993**, 799.
(37) Neese, F.; Petrenko, T.; Ganyushin, D.; Olbrich, G. *Coord. Chem. Rev.* **2007**, *251*, 288.
(38) Maurice, R.; Bastardis, R.; de Graaf, C.; Suaud, N.; Mallah, T.; Guihéry, N. *J. Chem. Theory Comput.* **2009**, *5*, 2977.
(39) Maurice, R.; Guihéry, N.; Bastardis, R.; de Graaf, C. *J. Chem. Theory Comput.* **2010**, *6*, 55; *erratum, ibid* **2010**, *6*, 977.
(40) Maurice, R.; Pradipto, A. M.; Guihéry, N.; Broer, R.; de Graaf, C. *J. Chem. Theory Comput.* **2010**, *6*, 3092.
(41) Maurice, R.; de Graaf, C.; Guihéry, N. *J. Chem. Phys.* **2010**, *133*, 084307.
(42) Atanasov, M.; Baerends, E. J.; Baettig, P.; Bruyndonckx, R.; Daul, C.; Rauzy, C.; Zbiri, M. *Chem. Phys. Lett.* **2004**, *399*, 433.
(43) McWeeny, R. *Methods of Molecular Quantum Mechanics*, 2nd ed.; Academic Press: New York, 1992.
(44) Jørgensen, C. K.; Pappalardo, R.; Schmidtke, H.-H. *J. Chem. Phys.* **1963**, *39*, 1422.
(45) Schäffer, C. E.; Jørgensen, C. K. *Mol. Phys.* **1965**, *9*, 401.
(46) Schönherr, T.; Atanasov, M.; Adamsky, H. *Comprehensive coordination chemistry*; Elsevier: New York, 2003; Vol. *II*., p 433.
(47) Figgis, B. N.; Hitchman, M. A. *Ligand Field Theory and its Applications*; Wiley-VCH: Weinheim, New York, 2000; p 354.
(48) Bridgeman, A. J.; Gerloch, M. *Prog. Inorg. Chem.* **1997**, *45*, 179.
(49) Comba, P. *Coord. Chem. Rev.* **1999**, *182*, 343.
(50) Hitchman, M. A. *Inorg. Chem.* **1972**, *11*, 2387.
(51) Bernhardt, P. V.; Comba, P. *Inorg. Chem.* **1993**, *32*, 2798.
(52) Comba, P.; Hambley, T. W.; Hitchman, M. A.; Stratemeier, H. *Inorg. Chem.* **1995**, *34*, 3903.
(53) Drickamer, H. G.; Frank, C. W. *Electronic Transitions and High Pressure Chemistry and Physics of Solids*; Chapman and Hall: London, 1973; p 174.

(54) Schäffer, C. E.; Lang, J. M.; Drickamer, H. G. *Inorg. Chem.* **1996**, *35*, 5072.
(55) Glerup, J.; Monsted, O.; Schäffer, C. E. *Inorg. Chem.* **1976**, *15*, 1399.
(56) Smith, D. W. *Inorg. Chem.* **1978**, *17*, 3153.
(57) Glerup, J.; Monsted, O.; Schäffer, C. E. *Inorg. Chem.* **1980**, *19*, 2855.
(58) Comba, P.; Nuber, B.; Ramlow, A. *J. Chem. Soc., Dalton Trans.* **1997**, 347.
(59) Lienke, A.; Klatt, G.; Robinson, D. J.; Koch, K. R.; Naidoo, K. J. *Inorg. Chem.* **2001**, *40*, 2352.
(60) Börzel, H.; Comba, P.; Hagen, K. S.; Kerscher, M.; Pritzkow, H.; Schatz, M.; Schindler, S.; Walter, O. *Inorg. Chem.* **2002**, *41*, 5440.
(61) Comba, P.; Merz, M.; Pritzkow, H. *Eur. J. Inorg. Chem.* **2003**, 1711.
(62) Bukowski, M. R.; Comba, P.; Lienke, A.; Limberg, C.; Lopez de Laorden, C.; Mas-Balleste, R.; Merz, M.; Que, L., Jr. *Angew. Chem., Int. Ed.* **2006**, *45*, 3446.
(63) Comba, P.; Wunderlich, S. *Chem.—Eur. J.* **2010**, *16*, 7293.
(64) Bridgeman, A. J.; Essex, S. J.; Gerloch, M. *Inorg. Chem.* **1994**, *34*, 5411.
(65) Pascal, P.; Pacault, A.; Hoarau, J. *C. R. Seances Acad. Sci.* **1951**, *233*, 1078.
(66) Sheldrick, G. M. *Acta Crystallogr.* **2008**, *A64*, 112.
(67) Sheldrick, G. M. *SHELXL-97*; University of Göttingen: Göttingen, Germany, 1997.
(68) Börzel, H.; Comba, P.; Hagen, K. S.; Merz, M.; Lampeka, Y. D.; Lienke, A.; Linti, G.; Pritzkow, H.; Tsymbal, L. V. *Inorg. Chim. Acta* **2002**, *337*, 407.
(69) Merz, K. W.; Haller, R. *Pharm. Acta Helv.* **1963**, *38*, 442.
(70) Caujolle, R.; Castera, P.; Lattes, A. *Bull. Soc. Chim. Fr.* **1984**, *9–10*, 413.
(71) Comba, P.; Lopez de Laorden, C.; Pritzkow, H. *Helv. Chim. Acta* **2005**, *88*, 647.

NOTE ADDED AFTER ASAP PUBLICATION

This paper was published on the Web on October 26, 2012, with minor errors in equations 7 and 8. The corrected version was reposted on November 5, 2012.